

A PARALLEL SOLVER FOR FSI PROBLEMS WITH FICTITIOUS DOMAIN APPROACH

DANIELE BOFFI, FABIO CREDALI, LUCIA GASTALDI, AND SIMONE SCACCHI

ABSTRACT. We present and analyze a parallel solver for the solution of fluid structure interaction problems described by a fictitious domain approach. In particular, the fluid is modeled by the non-stationary incompressible Navier–Stokes equations, while the solid evolution is represented by the elasticity equations. The parallel implementation is based on the PETSc library and the solver has been tested by running simulations on a Linux cluster.

Keywords: fluid-structure interactions, fictitious domain, preconditioners, parallel solver.

1. INTRODUCTION

In this work, we continue the analysis of the parallel solver for fluid structure interaction problems with fictitious domain approach, recently introduced in [7]. In particular, here we focus our attention on robustness with respect to mesh refinement, with different choices of time step, and weak scalability.

Our fictitious domain approach with distributed Lagrange multiplier was introduced in [5] as evolution of the immersed boundary method [11, 9]. The fluid is governed by the incompressible time dependent Navier–Stokes equations, while the immersed structure is characterized by linear and nonlinear constitutive laws. For the finite element discretization, we choose the (Q_2, P_1) element for velocity and pressure of the fluid and the Q_1 element for the structure variables; the time marching is a first order semi-implicit finite difference scheme. Moreover, the fluid-structure coupling matrix is assembled by exact computations over non-matching meshes as described in [6].

At each time step, the linear system arising from the discretization is solved by employing the GMRES method, combined with either a block-diagonal or a block-triangular preconditioner.

In Section 2 we present the mathematical model describing fluid structure interaction problems in the spirit of the fictitious domain approach. In Section 3, we describe the numerical method we implemented for our simulations and in Section 4 we introduce two possible choices of preconditioner for our parallel solver. Finally, in Section 5 we present some numerical tests in terms of robustness with respect to mesh refinement and weak scalability.

2. CONTINUOUS FORMULATION

We simulate fluid-structure interaction problems characterized by a visco-elastic incompressible solid body immersed in a viscous incompressible fluid. We denote by Ω_t^f and Ω_t^s the two regions in \mathbb{R}^d (with $d = 2, 3$) occupied by the fluid and the structure, respectively, at the time instant t ; the interface between these two regions is denoted by Γ_t . The evolution of such a system takes place inside Ω , that is the union of Ω_t^f and Ω_t^s : this new domain is independent of time and we assume

2020 *Mathematics Subject Classification.* 65N30, 65N12, 74F10, 65F08.

that it is connected and bounded with Lipschitz continuous boundary $\partial\Omega$. It is important to notice that, even if we are going to consider only thick solids, also the evolution of thin structures can be treated by our mathematical model.

The dynamics of the fluid is studied by considering the Eulerian description, associated with the variable \mathbf{x} . On the other hand, the evolution of the immersed body is modeled by Lagrangian description: we introduce the solid reference domain \mathcal{B} , associated with the variable \mathbf{s} , so that the deformation can be represented by the map $\mathbf{X} : \mathcal{B} \longrightarrow \Omega_t^s$. This means that $\mathbf{x} \in \Omega_t^s$ is the image of a certain point $\mathbf{s} \in \mathcal{B}$ at time t and the motion of the structure is represented by the kinematic equation

$$(1) \quad \mathbf{u}_s(\mathbf{x}, t) = \frac{\partial \mathbf{X}}{\partial t}(\mathbf{s}, t) \quad \text{for } \mathbf{x} = \mathbf{X}(\mathbf{s}, t),$$

denoting by \mathbf{u}_s the velocity. The deformation gradient $\nabla_s \mathbf{X}$ is denoted by \mathbb{F} and $J(\mathbf{s}, t) = \det \mathbb{F}(\mathbf{s}, t)$.

In our model, we consider a Newtonian fluid characterized by density ρ_f and viscosity $\nu_f > 0$, so that the Cauchy stress tensor can be written as

$$(2) \quad \boldsymbol{\sigma}_f = -p_f \mathbb{I} + \nu_f \underline{\boldsymbol{\varepsilon}}(\mathbf{u}_f),$$

where \mathbf{u}_f denotes the velocity of the fluid and p_f its pressure. In particular, the symbol $\underline{\boldsymbol{\varepsilon}}(\cdot)$ refers to the symmetric gradient $\underline{\boldsymbol{\varepsilon}}(\mathbf{v}) = (\nabla \mathbf{v} + \nabla \mathbf{v}^\top)/2$. Therefore, the dynamics in Ω_t^f is governed by the incompressible Navier–Stokes equations

$$(3) \quad \begin{aligned} \rho_f \left(\frac{\partial \mathbf{u}_f}{\partial t} + \mathbf{u}_f \cdot \nabla \mathbf{u}_f \right) &= \operatorname{div} \boldsymbol{\sigma}_f \\ \operatorname{div} \mathbf{u}_f &= 0. \end{aligned}$$

For the solid, we consider a viscous-hyperelastic material characterized by density ρ_s and viscosity $\nu_s > 0$; for this type of material, the Cauchy stress tensor $\boldsymbol{\sigma}_s$ can be seen as the sum of two contributions: a viscous part, similar to the one of the fluid

$$(4) \quad \boldsymbol{\sigma}_s^v = -p_s \mathbb{I} + \nu_s \underline{\boldsymbol{\varepsilon}}(\mathbf{u}_s),$$

and an elastic part which can be written in terms of the Piola–Kirchhoff stress tensor \mathbb{P}

$$(5) \quad \mathbb{P}(\mathbb{F}(\mathbf{s}, t)) = J(\mathbf{s}, t) \boldsymbol{\sigma}_s^e \mathbb{F}(\mathbf{s}, t)^{-\top} \quad \text{for } \mathbf{x} = \mathbf{X}(\mathbf{s}, t).$$

In particular, hyperelastic materials are characterized by a positive energy density $W(\mathbb{F})$ which is related with \mathbb{P} since $\mathbb{P}(\mathbb{F}) = \partial W / \partial \mathbb{F}$.

Finally, the system is described by the following equations in strong form

$$(6) \quad \begin{aligned} \rho_f \left(\frac{\partial \mathbf{u}_f}{\partial t} + \mathbf{u}_f \cdot \nabla \mathbf{u}_f \right) &= \operatorname{div} \boldsymbol{\sigma}_f && \text{in } \Omega_t^f \\ \operatorname{div} \mathbf{u}_f &= 0 && \text{in } \Omega_t^f \\ \rho_s \frac{\partial^2 \mathbf{X}}{\partial t^2} &= \operatorname{div} (J \boldsymbol{\sigma}_s^v \mathbb{F}^{-\top} + \mathbb{P}(\mathbb{F})) && \text{in } \mathcal{B} \\ \operatorname{div} \mathbf{u}_s &= 0 && \text{in } \Omega_t^s \end{aligned}$$

completed by two transmission conditions along the interface Γ_t

$$(7) \quad \begin{aligned} \mathbf{u}_f &= \mathbf{u}_s && \text{on } \Gamma_t \\ \boldsymbol{\sigma}_f \mathbf{n}_f &= -(\boldsymbol{\sigma}_s^v + J^{-1} \mathbb{P} \mathbb{F}^\top) \mathbf{n}_s && \text{on } \Gamma_t, \end{aligned}$$

where \mathbf{n}_f and \mathbf{n}_s denote the outer normals to Ω_t^f and Ω_t^s , respectively. Moreover, we consider the following initial and boundary conditions

$$(8) \quad \begin{aligned} \mathbf{u}_f(0) &= \mathbf{u}_{f,0} && \text{in } \Omega_0^f \\ \mathbf{u}_s(0) &= \mathbf{u}_{s,0} && \text{in } \Omega_0^s \\ \mathbf{X}(0) &= \mathbf{X}_0 && \text{in } \mathcal{B} \\ \mathbf{u}_f &= 0 && \text{on } \partial\Omega. \end{aligned}$$

The idea of the fictitious domain approach is to extend the first two equations in (6) to the whole domain Ω ; consequently, following [5], we introduce two new unknowns

$$(9) \quad \mathbf{u} = \begin{cases} \mathbf{u}_f & \text{in } \Omega_t^f \\ \mathbf{u}_s & \text{in } \Omega_t^s \end{cases} \quad p = \begin{cases} p_f & \text{in } \Omega_t^f \\ p_s & \text{in } \Omega_t^s. \end{cases}$$

In this new setting, (1) becomes a constraint on \mathbf{u} , since we have to impose that

$$(10) \quad \mathbf{u}(\mathbf{X}(\mathbf{s}, t), t) = \frac{\partial \mathbf{X}}{\partial t}(\mathbf{s}, t) \quad \text{for } \mathbf{s} \in \mathcal{B}.$$

This condition can be weakly enforced by employing a distributed Lagrange multiplier. To this end, we introduce a suitable functional space $\boldsymbol{\Lambda}$ and a continuous bilinear form \mathbf{c} such that

$$(11) \quad \begin{aligned} \mathbf{c} : \boldsymbol{\Lambda} \times H^1(\mathcal{B})^d &\longrightarrow \mathbb{R} \\ \mathbf{c}(\boldsymbol{\mu}, \mathbf{Y}) = 0 &\quad \forall \boldsymbol{\mu} \in \boldsymbol{\Lambda} \implies \mathbf{Y} = 0. \end{aligned}$$

We set \mathbf{c} to be the duality pairing between $H^1(\mathcal{B})^d$ and its dual $\boldsymbol{\Lambda} = (H^1(\mathcal{B})^d)'$, so that we have

$$(12) \quad \mathbf{c}(\boldsymbol{\mu}, \mathbf{Y}) = \langle \boldsymbol{\mu}, \mathbf{Y} \rangle \quad \forall \boldsymbol{\mu} \in (H^1(\mathcal{B})^d)', \forall \mathbf{Y} \in H^1(\mathcal{B})^d.$$

At this point, following [5, 8], the equations in (6), endowed with conditions (7) and (8), can be written in variational form.

For our simulations, we consider a simplified version of the problem: we assume that fluid ad solid materials have the same density, i.e $\rho_s = \rho_f$ and we drop the convective term of the Navier–Stokes equations.

Problem 1. Given $\mathbf{u}_0 \in H_0^1(\Omega)^d$ and $\mathbf{X}_0 \in W^{1,\infty}(\mathcal{B})$, find $\mathbf{u}(t) \in H_0^1(\Omega)^d$, $p(t) \in L_0^2(\Omega)$, $\mathbf{X}(t) \in H^1(\mathcal{B})^d$, and $\boldsymbol{\lambda}(t) \in \boldsymbol{\Lambda}$ such that for almost all $t \in (0, T)$:

$$\begin{aligned}
& \rho_f \left(\frac{\partial}{\partial t} \mathbf{u}(t), \mathbf{v} \right)_\Omega + a(\mathbf{u}(t), \mathbf{v}) \\
& \quad - (\operatorname{div} \mathbf{v}, p(t))_\Omega + \langle \boldsymbol{\lambda}(t), \mathbf{v}(\mathbf{X}(\cdot, t)) \rangle = 0 \quad \forall \mathbf{v} \in H_0^1(\Omega)^d \\
& (\operatorname{div} \mathbf{u}(t), q)_\Omega = 0 \quad \forall q \in L_0^2(\Omega) \\
& (\mathbb{P}(\mathbb{F}(t)), \nabla_s \mathbf{Y})_\mathcal{B} - \langle \boldsymbol{\lambda}(t), \mathbf{Y} \rangle = 0 \quad \forall \mathbf{Y} \in H^1(\mathcal{B})^d \\
& \langle \boldsymbol{\mu}, \mathbf{u}(\mathbf{X}(\cdot, t), t) - \frac{\partial \mathbf{X}}{\partial t}(t) \rangle = 0 \quad \forall \boldsymbol{\mu} \in \boldsymbol{\Lambda} \\
& \mathbf{u}(\mathbf{x}, 0) = \mathbf{u}_0(\mathbf{x}) \quad \text{in } \Omega \\
& \mathbf{X}(\mathbf{s}, 0) = \mathbf{X}_0(\mathbf{s}) \quad \text{in } \mathcal{B}.
\end{aligned}$$

In particular, $a(\mathbf{u}, \mathbf{v}) = \nu(\underline{\varepsilon}(\mathbf{u}), \underline{\varepsilon}(\mathbf{v}))_\Omega$, where ν is the extended viscosity with value ν_f in Ω_t^f and ν_s in Ω_t^s .

3. DISCRETE FORMULATION

Before discussing the discrete formulation, we remark that, from now on, we focus on two dimensional problems ($d = 2$).

The time semi-discretization of Problem 1 is based on the Backward Euler scheme. The time interval $[0, T]$ is partitioned into N parts with uniform size $\Delta t = T/N$. We denote the subdivision nodes by $t_n = n\Delta t$. For a generic function g depending on time, setting $g^n = g(t_n)$, the time derivative is approximated as

$$(13) \quad \frac{\partial g}{\partial t}(t_{n+1}) \approx \frac{g^{n+1} - g^n}{\Delta t}.$$

Therefore, we obtain a semi-implicit first order scheme in time.

On the other hand, for the discretization in space, we work with quadrilateral meshes for both fluid and solid.

For the fluid, we consider a mesh \mathcal{T}_h^Ω for Ω with meshsize h_Ω . We then consider two finite element spaces $\mathbf{V}_h \subset H_0^1(\Omega)^d$ and $Q_h \subset L_0^2(\Omega)$ for velocity and pressure, respectively, satisfying the inf-sup condition for the Stokes problem. In particular, we work with the $(\mathcal{Q}_2, \mathcal{P}_1)$ pair.

On the other hand, for \mathcal{B} , we choose a mesh $\mathcal{T}_h^\mathcal{B}$ with meshsize $h_\mathcal{B}$, independent from \mathcal{T}_h^Ω . We then consider two finite dimensional spaces $\mathbf{S}_h \subset H^1(\mathcal{B})^d$ and $\boldsymbol{\Lambda}_h \subset \boldsymbol{\Lambda}$. We assume that $\mathbf{S}_h = \boldsymbol{\Lambda}_h$ and we approximate both variables \mathbf{X} and Lagrange multiplier with piecewise bilinear elements on quadrilaterals.

We notice that, since $\boldsymbol{\Lambda}_h$ is included in $L^2(\mathcal{B})^d$, at discrete level the coupling bilinear form \mathbf{c} can be replaced by the scalar product in $L^2(\mathcal{B})^d$

$$(14) \quad \mathbf{c}(\boldsymbol{\mu}_h, \mathbf{Y}_h) = (\boldsymbol{\mu}_h, \mathbf{Y}_h)_\mathcal{B} \quad \forall \boldsymbol{\mu}_h \in \boldsymbol{\Lambda}_h \forall \mathbf{Y}_h \in \mathbf{S}_h.$$

Therefore, we get the following full discretized problem.

Problem 2. Given $\mathbf{u}_{0,h} \in \mathbf{V}_h$ and $\mathbf{X}_{0,h} \in \mathbf{S}_h$, for all $n = 1, \dots, N$ find $\mathbf{u}_h^n \in \mathbf{V}_h$, $p_h^n \in Q_h$, $\mathbf{X}_h^n \in \mathbf{S}_h$, and $\boldsymbol{\lambda}_h^n \in \boldsymbol{\Lambda}_h$ fulfilling:

$$\begin{aligned}
& \rho_f \left(\frac{\mathbf{u}_h^{n+1} - \mathbf{u}_h^n}{\Delta t}, \mathbf{v}_h \right)_\Omega + a(\mathbf{u}_h^{n+1}, \mathbf{v}_h) \\
& \quad - (\operatorname{div} \mathbf{v}_h, p_h^{n+1})_\Omega + (\boldsymbol{\lambda}_h^{n+1}, \mathbf{v}_h(\mathbf{X}_h^n))_{\mathcal{B}} = 0 \quad \forall \mathbf{v}_h \in \mathbf{V}_h \\
& (\operatorname{div} \mathbf{u}_h^{n+1}, q_h)_\Omega = 0 \quad \forall q_h \in Q_h \\
& (\mathbb{P}(\mathbb{F}_h^{n+1}), \nabla_s \mathbf{Y}_h)_{\mathcal{B}} - (\boldsymbol{\lambda}_h^{n+1}, \mathbf{Y}_h)_{\mathcal{B}} = 0 \quad \forall \mathbf{Y}_h \in \mathbf{S}_h \\
& \left(\boldsymbol{\mu}_h, \mathbf{u}_h^n(\mathbf{X}_h^n) - \frac{\mathbf{X}_h^{n+1} - \mathbf{X}_h^n}{\Delta t} \right)_{\mathcal{B}} = 0 \quad \forall \boldsymbol{\mu}_h \in \boldsymbol{\Lambda}_h \\
& \mathbf{u}_h^0 = \mathbf{u}_{0,h}, \quad \mathbf{X}_h^0 = \mathbf{X}_{0,h}.
\end{aligned}$$

Assuming for simplicity $\mathbb{P}(\mathbb{F}) = \kappa \mathbb{F}$, Problem 2 can be represented in matrix form as

$$(15) \quad \left[\begin{array}{cc|cc} \mathbf{A}_f & -\mathbf{B}^\top & 0 & \mathbf{C}_f(\mathbf{X}_h^n)^\top \\ -\mathbf{B} & 0 & 0 & 0 \\ \hline 0 & 0 & \mathbf{A}_s & -\mathbf{C}_s^\top \\ \mathbf{C}_f(\mathbf{X}_h^n) & 0 & -\frac{1}{\Delta t} \mathbf{C}_s & 0 \end{array} \right] \begin{bmatrix} \mathbf{u}_h^{n+1} \\ p_h^{n+1} \\ \mathbf{X}_h^{n+1} \\ \lambda_h^{n+1} \end{bmatrix} = \begin{bmatrix} \mathbf{g}_1 \\ 0 \\ 0 \\ \mathbf{g}_2 \end{bmatrix},$$

with

$$\begin{aligned}
\mathbf{A}_f &= \frac{\rho_f}{\Delta t} \mathbf{M}_f + \mathbf{K}_f \\
(\mathbf{M}_f)_{ij} &= (\phi_j, \phi_i)_\Omega, \quad (\mathbf{K}_f)_{ij} = a(\phi_j, \phi_i) \\
\mathbf{B}_{ki} &= (\operatorname{div} \phi_i, \psi_k)_\Omega \\
(\mathbf{A}_s)_{ij} &= \kappa (\nabla_s \chi_j, \nabla_s \chi_i)_{\mathcal{B}} \\
(\mathbf{C}_f(\mathbf{X}_h^n))_{\ell j} &= (\chi_\ell, \phi_j(\mathbf{X}_h^n))_{\mathcal{B}}, \quad (\mathbf{C}_s)_{\ell j} = (\chi_\ell, \chi_j)_{\mathcal{B}} \\
\mathbf{g}_1 &= \frac{\rho_f}{\Delta t} \mathbf{M}_f \mathbf{u}_h^n, \quad \mathbf{g}_2 = -\frac{1}{\Delta t} \mathbf{C}_s \mathbf{X}_h^n.
\end{aligned}$$

In particular, ϕ_i and ψ_k denote the basis functions for \mathbf{V}_h and Q_h respectively, while χ_j are the basis functions for the space defined on \mathcal{B} . We observe that, due to our choices, \mathbf{C}_s represents a mass matrix.

We can observe that the matrix in (15) splits into four blocks, defined as follows:

$$\begin{aligned}
\mathcal{A}_{11} &= \begin{bmatrix} \mathbf{A}_f & -\mathbf{B}^\top \\ -\mathbf{B} & 0 \end{bmatrix} \quad \mathcal{A}_{12} = \begin{bmatrix} 0 & \mathbf{C}_f(\mathbf{X}_h^n)^\top \\ 0 & 0 \end{bmatrix} \\
\mathcal{A}_{21} &= \begin{bmatrix} 0 & 0 \\ \mathbf{C}_f(\mathbf{X}_h^n) & 0 \end{bmatrix} \quad \mathcal{A}_{22} = \begin{bmatrix} \mathbf{A}_s & -\mathbf{C}_s^\top \\ -\frac{1}{\Delta t} \mathbf{C}_s & 0 \end{bmatrix}
\end{aligned}$$

where \mathcal{A}_{11} is related to the fluid dynamic, \mathcal{A}_{22} to the solid evolution, while \mathcal{A}_{12} and \mathcal{A}_{21} contain the coupling term.

Particular attention has to be paid to the assembly of the coupling matrix $\mathbf{C}_f(\mathbf{X}_h^n)$, since it involves the integration over \mathcal{B} of solid and fluid basis functions, taking into account the position of Ω_t^s . For more details about the procedure in a similar situation, we refer to [6]. In particular, we implement an exact quadrature rule by computing, at each time step, the intersection between the fluid mesh \mathcal{T}_h^Ω and the mapped solid mesh $\mathbf{X}_h^n(\mathcal{T}_h^\mathcal{B})$.

In general, when $\mathbb{P}(\mathbb{F})$ is nonlinear, the system is solved making use of the Newton iterator method.

4. PARALLEL PRECONDITIONERS

The design of an efficient parallel solver influences two aspects of the numerical method: firstly, the finite element matrices need to be assembled in parallel on each processor and, secondly, the solution of the saddle point system arising from the discretization has to be solved saving computational resources, in terms of both memory and execution time. For this purpose, we implemented a Fortran90 code based on the library PETSc [4, 3].

We introduce two possible choices of preconditioner:

- *block-diagonal preconditioner*

$$\begin{bmatrix} \mathcal{A}_{11} & 0 \\ 0 & \mathcal{A}_{22} \end{bmatrix}$$

- *block-triangular preconditioner*

$$\begin{bmatrix} \mathcal{A}_{11} & 0 \\ \mathcal{A}_{21} & \mathcal{A}_{22} \end{bmatrix}.$$

We solve the linear system making use of the parallel GMRES method combined with the action of our preconditioners, which consists in the exact inversion of the diagonal blocks performed by the parallel direct solver Mumps [1, 2].

5. NUMERICAL TESTS

The proposed preconditioners have been widely studied in [7] in terms of robustness with respect to mesh refinement, strong scalability and refinement of the time step. In this work, after reporting new results in terms of optimality, we analyze the weak scalability of our solver. We focus on both linear and nonlinear models describing the solid material.

The simulations have been run on the Shaheen cluster at King Abdullah University of Science and Technology (KAUST, Saudi Arabia). It is a Cray XC40 cluster constituted by 6,174 dual sockets compute nodes, based on 16 core Intel Haswell processors running at 2.3GHz. Each node has 128GB of DDR4 memory running at 2300MHz.

5.1. Linear solid model. We consider the quarter of the elastic annulus $\{\mathbf{x} \in \mathbb{R}^2 : 0.3 \leq |\mathbf{x}| \leq 0.5\}$ included in $\Omega = [0, 1]^2$: in particular, the solid reference domain corresponds to the resting configuration of the body, that is

$$\mathcal{B} = \{\mathbf{s} = (s_1, s_2) \in \mathbb{R}^2 : s_1, s_2 \geq 0, 0.3 \leq |\mathbf{s}| \leq 0.5\}.$$

The dynamics of the system is generated by stretching the annulus and observing how internal forces bring it back to the resting condition. In this case, Ω_0^s coincides with the stretched annulus. Four snapshots of the evolution are shown in Figure 1.

The solid behavior is governed by a linear model, therefore $\mathbb{P}(\mathbb{F}) = \kappa \mathbb{F}$, with $\kappa = 10$. We choose fluid and solid materials with same density $\rho_f = \rho_s = 1$ and same viscosity $\nu_f = \nu_s = 0.1$. We impose no slip conditions for the velocity on the upper and right edge of Ω , while on the other two

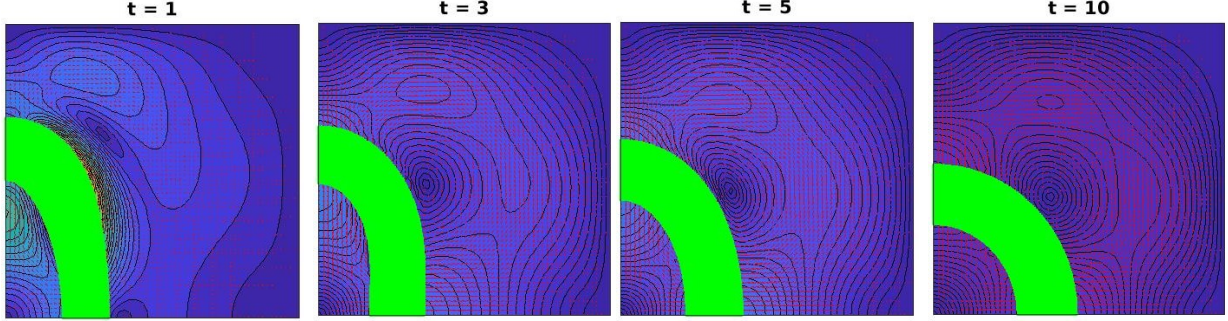


FIGURE 1. Four snapshots of the evolution of the structure with linear constitutive law.

edges, we allow the motion of both fluid and structure along the tangential direction. Finally, the following initial conditions are considered

$$\mathbf{u}(\mathbf{x}, 0) = 0, \quad \mathbf{X}(\mathbf{s}, 0) = \left(\frac{s_1}{1.4}, 1.4 s_2 \right).$$

In Table 1, we report the results for the optimality test, where the robustness of the solver is studied by refining the mesh and keeping fixed the number of processors. In particular, we set the time step $\Delta t = 0.01$ and the final time of simulation $T = 2$. The number of processors used for the simulation is 32. The time T_{ass} needed to assemble the matrix of the problem increases moderately, while the time T_{coup} , needed for the assembly of the coupling matrix by computing the intersection between the involved meshes, exhibits a superlinear growth. In terms of preconditioners, we can see that block-diag is not robust with respect to mesh refinement since the number of GMRES iterations grows from 13 to 430; clearly, this phenomenon affects also the time T_{sol} we need to solve the system. On the other hand, block-tri is robust since the number of GMRES iterations remains bounded by 14 when the mesh is refined. Therefore, T_{sol} presents only a moderate growth and, for 1074054 dofs, it is 30 times smaller than the value we get for block-diag preconditioner.

The weak scalability of the proposed parallel solver is analyzed in Table 2. Again, we choose $T = 2$ and $\Delta t = 0.01$. We perform six tests by doubling both the global number of dofs and the number of processors. Thanks to the resources provided by PETSc, the time T_{ass} to assemble stiffness and mass matrices is perfectly scalable. On the other hand, the assembly procedure for the coupling matrix is much more complicated: to detect all the intersections between solid and fluid elements, the algorithm consists of two nested loops. For each solid element (outer loop), we check its position with respect to all the fluid elements (inner loop). In particular, only the outer loop is distributed over all the processors. Consequently, T_{coup} is not scalable since the number of fluid dofs, analyzed in serial, increases at each test. We now discuss the behavior of the two proposed preconditioners. It is evident that block-diag is not scalable since the number of GMRES iteration drastically increases as we increase dofs and procs, clearly affecting T_{sol} and T_{tot} . On the other hand, block-tri behaves well: even if it is not perfectly scalable, the number of iterations slightly increases from 8 to 18 and T_{sol} ranges from $2.24 \cdot 10^{-1} s$ to $11.43 s$.

5.2. Nonlinear solid model. For this test, we set again the fluid domain Ω to be the unit square. On the other hand, the immersed solid body is a bar represented, at resting configuration, by the

Linear solid model – Mesh refinement test								
procs = 32, T = 2, $\Delta t = 0.01$								
dofs	$T_{ass}(s)$	$T_{coup}(s)$	block-diag			block-tri		
			its	$T_{sol}(s)$	$T_{tot}(s)$	its	$T_{sol}(s)$	$T_{tot}(s)$
30534	1.02e-2	9.98e-2	13	1.14e-1	42.01	7	6.93e-2	33.83
120454	2.12e-2	1.09	31	8.30e-1	390.90	9	2.40e-1	266.17
269766	9.20e-2	7.60	97	5.41	2.55e+3	11	6.47e-1	1.65e+3
478470	1.31e-1	25.04	192	18.75	9.07e+3	12	1.14	5.24e+3
746566	1.23e-1	85.32	422	67.92	3.07e+4	13	2.17	1.75e+4
1074054	1.81e-1	196.88	430	97.19	5.90e+4	14	3.21	4.00e+4

TABLE 1. Refining the mesh in the linear solid model. The simulations are run on the Shaheen cluster. procs = number of processors; dofs = degrees of freedom; T_{ass} = CPU time to assemble the stiffness and mass matrices; T_{coup} = CPU time to assemble the coupling term; its = GMRES iterations; T_{sol} = CPU time to solve the linear system; T_{tot} = total simulation CPU time. The quantities T_{coup} , its and T_{sol} are averaged over the time steps. All CPU times are reported in seconds.

Linear solid model – Weak scalability test								
T = 2, $\Delta t = 0.01$								
procs	dofs	$T_{ass}(s)$	$T_{coup}(s)$	block-diag			block-tri	
				its	$T_{sol}(s)$	$T_{tot}(s)$	its	$T_{sol}(s)$
4	68070	8.55e-2	3.95	22	6.25e-1	933.43	8	2.24e-1
8	135870	1.00e-1	5.23	38	2.16	1.48e+3	9	4.41e-1
16	269766	1.01e-1	8.77	111	10.23	3.80e+3	11	9.70e-1
32	539926	9.24e-2	59.27	706	108.05	2.50e+4	18	2.91
64	1074054	1.90e-1	48.00	429	113.59	3.24e+4	14	3.90
128	2152614	1.90e-1	98.63	-	-	-	18	11.43
								2.20e+4

TABLE 2. Weak scalability for the linear solid model. The simulations are run on the Shaheen cluster. Same format as Table 1.

rectangle $\mathcal{B} = \Omega_0^s = [0, 0.4] \times [0.45, 0.55]$. During the time interval $[0, 1]$, the structure is pulled down by a force applied at the middle point of the right edge. Therefore, when it is released, the solid body returns to its resting configuration by the action of internal forces. Four snapshots of the evolution are shown in Figure 2.

The energy density of the solid material is given by the potential strain energy function of an isotropic hyperelastic material; in particular, we have

$$W(\mathbb{F}) = (\gamma/2\eta) \exp(\eta \operatorname{tr}(\mathbb{F}^\top \mathbb{F}) - 2),$$

where $\operatorname{tr}(\mathbb{F}^\top \mathbb{F})$ denotes the trace of $\mathbb{F}^\top \mathbb{F}$, while $\gamma = 1.333$ and $\eta = 9.242$.

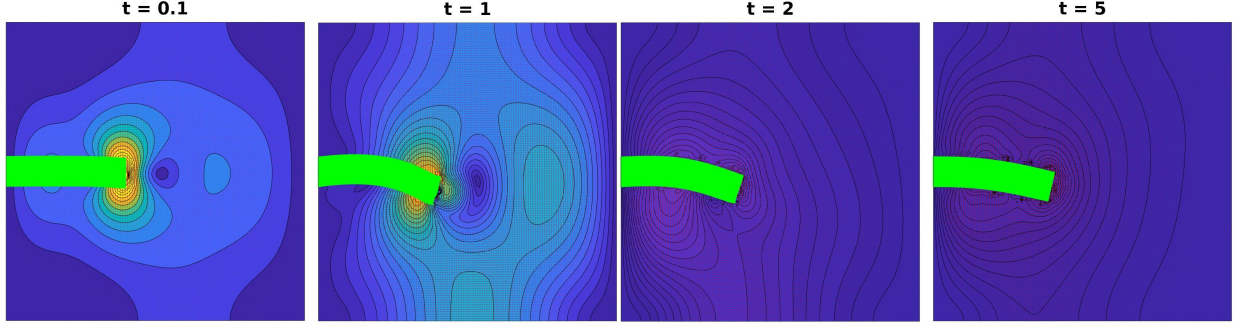


FIGURE 2. Four snapshots of the evolution of the structure with nonlinear constitutive law.

Also for this test we assume that fluid and solid materials share the same density, equal to 1, and the same viscosity, equal to 0.2. The velocity is imposed to be zero at the boundary of Ω , while the following initial conditions are imposed

$$\mathbf{u}(\mathbf{x}, 0) = 0, \quad \mathbf{X}(\mathbf{s}, 0) = \mathbf{s}.$$

Results for the mesh refinement test are reported in Table 3: we consider the evolution of the system during the time interval $[0, 2]$, with time step $\Delta t = 0.002$. The number of processors for the simulations is set to be 64, while the number of dofs increases from 21222 to 741702. As for the linear case, T_{ass} increases moderately and T_{coup} follows a superlinear growth. Both preconditioners are robust with respect to mesh refinement: the number of Newton iterations is 2 for each test and the average number of GMRES iterations per nonlinear iteration is bounded by 15 for block-diag and by 10 for block-tri. This behavior of block-diag is in contrast with the results we obtained for the linear solid model: this is due to the finer time step chosen for this simulation.

To study the weak scalability, we choose $T = 0.1$ and $\Delta t = 0.002$. The results, reported in Table 4, are similar to the results obtained for the linear case. As before, T_{coup} is not scalable due to the algorithm we implemented for assembling the coupling term. Even if it is not perfectly scalable, block-tri performs pretty well since the average number of linear iterations per nonlinear iteration increases only from 15 to 19. On the other hand, the good behavior of block-diag registered in Table 3 is not confirmed: the average number of linear iterations reaches 101, showing a lack of weak scalability as already seen in Table 2.

6. CONCLUSIONS

We analyzed two preconditioners, block-diagonal and block-triangular, for saddle point systems originating from the finite element discretization of fluid-structure interaction problems with fictitious domain approach. In particular, the analysis has been done by studying the robustness with respect to mesh refinement and weak scalability, applying the parallel solver to both linear and nonlinear problems.

Only block-triangular appears to be robust in terms of mesh refinement for linear and nonlinear problems; on the other hand, block-diagonal works well when the time step is very small.

Moreover, by studying the weak scalability, we can notice two further limitations of the proposed method, which will be the subject of future studies. First, the time to assemble the coupling matrix

Nonlinear solid model – Mesh refinement test										
procs = 64, T = 2, $\Delta t = 0.002$										
dofs	$T_{ass}(s)$	$T_{coup}(s)$	block-diag				block-tri			
			nit	its	$T_{sol}(s)$	$T_{tot}(s)$	nit	its	$T_{sol}(s)$	$T_{tot}(s)$
21222	4.04e-3	3.89e-2	2	11	4.29e-1	9.35e+2	2	8	3.93e-1	8.64e+2
83398	1.68e-2	3.60e-1	2	12	1.67	4.06e+3	2	8	1.57	3.86e+3
186534	3.80e-2	1.57	2	14	4.23	1.16e+4	2	9	4.00	1.11e+4
330630	6.68e-2	4.77	2	14	7.71	2.49e+4	2	10	7.07	2.37e+4
515686	1.05e-1	11.40	2	15	13.03	4.92e+4	2	10	11.48	4.58e+4
741702	1.52e-1	23.23	2	15	18.58	8.49e+4	2	10	16.63	7.98e+4

TABLE 3. Refining the mesh in the nonlinear solid model. The simulations are run on the Shaheen cluster. procs = number of processors; dofs = degrees of freedom; T_{ass} = CPU time to assemble the stiffness and mass matrices; T_{coup} = CPU time to assemble the coupling term; nit = Newton iterations; its = GMRES iterations to solve the Jacobian system; T_{sol} = CPU time to solve the Jacobian system; T_{tot} = total simulation CPU time. The quantities T_{coup} and nit are averaged over the time steps, whereas the quantities its and T_{sol} are averaged over the Newton iterations and the time steps. All CPU times are reported in seconds.

Nonlinear solid model – Weak scalability test											
T = 0.1, $\Delta t = 0.002$											
procs	dofs	$T_{ass}(s)$	$T_{coup}(s)$	block-diag				block-tri			
				nit	its	$T_{sol}(s)$	$T_{tot}(s)$	nit	its	$T_{sol}(s)$	$T_{tot}(s)$
4	83398	1.01e-1	2.21	3	23	6.76	448.65	3	15	5.50	386.13
8	156910	1.59e-1	3.77	3	38	15.49	963.03	3	16	8.87	627.84
16	330630	1.62e-1	8.92	3	49	36.58	2.28e+3	3	17	17.84	1.34e+3
32	741702	2.60e-1	25.18	3	67	123.99	7.46e+3	3	18	48.85	3.70e+3
64	1316614	2.61e-1	69.12	3	101	328.18	1.99e+4	3	19	97.28	8.38e+3

TABLE 4. Weak scalability for the nonlinear solid model. The simulations are run on the Shaheen cluster. Same format as Table 3.

is not scalable: it is based on two nested loops, on solid and fluid elements respectively; but only the external one is done in parallel over the processors. Second, since the action of the preconditioners consists of the exact inversion of two matrices, the time for solving the linear system slightly increases when the mesh is refined.

ACKNOWLEDGMENTS

The authors are member of INdAM Research group GNCS. D. Boffi, F. Credali and L. Gastaldi are partially supported by IMATI/CNR. Moreover, D. Boffi and L. Gastaldi are partially supported by PRIN/MIUR.

REFERENCES

- [1] P. R. Amestoy, I. S. Duff, J.-Y. L'Excellent, and J. Koster. A fully asynchronous multifrontal solver using distributed dynamic scheduling. *SIAM J. Matr. Anal. Appl.*, 23(1):15–41, 2001.
- [2] P. R. Amestoy, A. Guermouche, J.-Y. L'Excellent, and S. Pralet. Hybrid scheduling for the parallel solution of linear systems. *Paral. Comput.*, 32(2):136–156, 2006.
- [3] S. Balay, S. Abhyankar, M. F. Adams, J. Brown, P. Brune, K. Buschelman, L. Dalcin, V. Eijkhout, W. D. Gropp, D. Kaushik, M. G. Knepley, D. A. May, L. C. McInnes, R. T. Mills, T. Munson, K. Rupp, P. Sanan, B. F. Smith, S. Zampini, H. Zhang, and H. Zhang. PETSc users manual. Technical Report ANL-95/11 - Revision 3.9, Argonne National Laboratory, 2018.
- [4] S. Balay, S. Abhyankar, M. F. Adams, J. Brown, P. Brune, K. Buschelman, L. Dalcin, V. Eijkhout, W. D. Gropp, D. Kaushik, M. G. Knepley, D. A. May, L. C. McInnes, R. T. Mills, T. Munson, K. Rupp, P. Sanan, B. F. Smith, S. Zampini, H. Zhang, and H. Zhang. PETSc Web page. <http://www.mcs.anl.gov/petsc>, 2018.
- [5] D. Boffi, N. Cavallini, and L. Gastaldi. The finite element immersed boundary method with distributed lagrange multiplier. *SIAM J. Numer. Anal.*, 53(6):2584–2604, 2015.
- [6] D. Boffi, F. Credali, and L. Gastaldi. On the interface matrix for fluid–structure interaction problems with fictitious domain approach. *Computer Methods in Applied Mechanics and Engineering*, 401:115650, 2022.
- [7] D. Boffi, F. Credali, L. Gastaldi, and S. Scacchi. A parallel solver for fluid structure interaction problems with lagrange multiplier. *arXiv preprint arXiv:2212.13410*, 2022.
- [8] D. Boffi and L. Gastaldi. A fictitious domain approach with lagrange multiplier for fluid-structure interactions. *Numer. Math.*, 135(3):711–732, 2017.
- [9] D. Boffi, L. Gastaldi, L. Heltai, and C. S. Peskin. On the hyper-elastic formulation of the immersed boundary method. *Computer Methods in Applied Mechanics and Engineering*, 197(25–28):2210–2231, 2008.
- [10] J. L. Lions and E. Magenes. *Non-homogeneous boundary value problems and applications: Vol. 1*, volume 181. Springer Science & Business Media, 2012.
- [11] C. S. Peskin. The immersed boundary method. *Acta numerica*, 11:479–517, 2002.

COMPUTER, ELECTRICAL AND MATHEMATICAL SCIENCES AND ENGINEERING DIVISION, KING ABDULLAH UNIVERSITY OF SCIENCE AND TECHNOLOGY, THUWAL 23955, SAUDI ARABIA AND DIPARTIMENTO DI MATEMATICA “F. CASORATI”, UNIVERSITÀ DEGLI STUDI DI PAVIA, VIA FERRATA 1, 27100, PAVIA, ITALY

Email address: daniele.boffi@kaust.edu.sa

URL: kaust.edu.sa/en/study/faculty/daniele-boffi

COMPUTER, ELECTRICAL AND MATHEMATICAL SCIENCES AND ENGINEERING DIVISION, KING ABDULLAH UNIVERSITY OF SCIENCE AND TECHNOLOGY, THUWAL 23955, SAUDI ARABIA AND DIPARTIMENTO DI MATEMATICA “F. CASORATI”, UNIVERSITÀ DEGLI STUDI DI PAVIA, VIA FERRATA 1, 27100, PAVIA, ITALY

Email address: fabio.credali@kaust.edu.sa

URL: cemse.kaust.edu.sa/amcs/people/person/fabio-credali

DIPARTIMENTO DI INGEGNERIA CIVILE, ARCHITETTURA, TERRITORIO, AMBIENTE E DI MATEMATICA, UNIVERSITÀ DEGLI STUDI DI BRESCIA, VIA BRANZE 43, 25123, BRESCIA, ITALY

Email address: lucia.gastaldi@unibs.it

URL: lucia-gastaldi.unibs.it

DIPARTIMENTO DI MATEMATICA “F. ENRIQUES”, UNIVERSITÀ DEGLI STUDI DI MILANO, VIA SALDINI 50, 20133 MILANO, ITALY

Email address: simone.scacchi@unimi.it

URL: mat.unimi.it/users/scacchi/